Towards Electrochemical Fabrication of Free-Standing Indium Phosphide Nanofilms

Nathan Quill,[a] Colm O'Dwyer,[b] D. Noel Buckley [a] and Robert P. Lynch [a,†]

[a] Department of Physics & Energy, and Materials & Surface Science Institute, University of Limerick, Ireland
[b] Department of Chemistry, and Tyndall National Institute, University College Cork, Ireland

Abstract

The formation of sub-surface truncated tetrahedral voids beneath suspended ~40 nm thick dense InP shelves is achievable via a two-step etching method. The first step involves the electrochemical anodisation of n-type InP in aqueous KOH electrolyte resulting in the formation of truncated tetrahedral domains of pores beneath an ~40 nm thick dense surface layer with an individual pit that penetrates the dense surface layer of each domain. The second step involves the preferential chemical etching of these porous domains with only limited etching of the surrounding bulk InP and dense surface layer. The resulting structure of each domain is a truncated tetrahedral void with a dense InP layer suspended above it. This new technique may be a very useful tool in the fabrication of devices based on III-V semiconductors and it may be possible to extend the technique to the fabrication of free-standing InP nanofilms.

Introduction

III-V semiconductors have received considerable research attention due to their use in the optoelectronics industry. In recent years, particular interest has been paid to the fabrication and characterisation of nano-scale structures for various applications. Nanopore formation due to electrochemical etching has been demonstrated in a range of semiconductors from Si to InP(1-12). The morphology of these porous layers can vary wildly between different semiconductors(13), and for an individual semiconductor with the variation of temperature(14), composition(15, 16) and concentration(17) of electrolyte, and orientation(18) and doping density(19) of the substrate. Many different pore morphologies have been observed and several models have been proposed(20-32) to explain them. However, it is generally accepted that the propagation of nanopores in highly doped n-type semiconductors is controlled by hole generation under the influence of a high electric field due to the small radius of curvature at the pore tip(29, 30).

We have previously investigated(14,15,33-39) the early stages of pore formation in InP in aqueous KOH electrolytes. Pores originate from etch pits in the electrode surface and propagate along <111>A directions to form porous domains beneath a thin dense (*i.e.* low

† E-mail: Robert.Lynch@UL.ie

porosity) surface layer penetrated only by the surface pits(35). The domains shape is that of a truncated tetrahedron due to the preferential growth direction of the individual pores. Eventually these domains merge to create a continuous porous layer(39).

There have been a number of applications proposed for the various porous structures that can be formed(40-53) in different semiconductors under different conditions. In this paper we demonstrate how the porous InP domains that we have previously characterised can be chemically etched, leaving behind a unique structure: a truncated tetrahedron shaped void, below the dense surface layer which is ~40 nm thick and freely suspended above the void.

Experimental

Wafers were monocrystalline, sulfur-doped, n-type indium phosphide (n-InP) grown by the liquid-encapsulated Czochralski (LEC) method and supplied by Sumitomo Electric. They were polished on one side and had a surface orientation of (100) and a carrier concentration in the range $3–7 \times 10^{18}$ cm^{-3}. To fabricate working electrodes, wafers were cleaved into coupons along the natural {011} cleavage planes. Ohmic contact was made by alloying indium to the back of a coupon. The electrodes were cleaned by rinsing and then immersion in firstly acetone, then methanol and finally water. The back and the cleaved edges were then isolated from the electrolyte by means of a suitable varnish. The electrode area was typically 0.2 cm^2. Prior to immersion in the electrolyte, the working electrode was immersed in a piranha etchant (3:1:1 H_2SO_4:H_2O_2:H_2O) for 4 minutes and then rinsed with deionized water.

As described previously(14,15,33-39) anodisation was carried out in aqueous 5 mol dm^{-3} KOH electrolytes in the absence of light at room temperature ~19°C using a linear potential sweep (LPS). A conventional three-electrode cell configuration was used, employing a platinum counter electrode and a saturated calomel electrode (SCE) to which all potentials are referenced. LPSs were carried out at 2.5 mV s^{-1} from 0.0 V to an E_{max}. A CH Instruments Model 650A Electrochemical Workstation interfaced to a Personal Computer (PC) was employed for cell parameter control and for data acquisition.

Cleaved $(0\bar{1}1)$ and $(0\bar{1}\bar{1})$ cross sections of electrodes were examined using a Hitachi S-4800 field-emission scanning electron microscope (FE SEM) operating at 5 kV, unless otherwise stated.

Results and Discussion

Formation of Unique Porous Structure

We have previously reported the formation of porous layers in n-InP that has been anodised in > 2 mol dm^{-3} KOH solutions(14,15,33-39). A typical linear sweep voltammogram (LSV) obtained during the potentiodynamic formation of porous InP in 5 mol dm^{-3} KOH is shown in Fig. 1. On the plot, three potentials are labelled: E_{pit}, the pitting potential, E_{p1}, the potential of the first current peak, and E_{p2}, the potential of the second current peak. Since a depletion layer exists at the n-InP surface under the

conditions required for pore formation, the etch rate is generally limited by hole supply at the semiconductor surface. In the absence of illumination or a highly oxidising species within the electrolyte, these holes must be generated within the bulk semiconductor. In order for these holes to reach the surface of the semiconductor and facilitate etching, they must cross the depletion layer at the surface. The electric field enhancement that occurs at a sharp etch pit or pore tip(29, 30) can be sufficient to allow a hole to tunnel across the depletion layer once the potential drop across the depletion layer is sufficiently large. For this reason, at potentials below E_{pit}, no significant current flows and no significant electrode modification takes place.

As the current begins to increase at potentials greater than E_{pit}, etch pits begin to appear in the electrode surface. Figure 2 shows an SEM image of the (100) surface (the surface exposed to the electrolyte) of a porous InP sample. A number of these etch pits can be seen penetrating the InP surface. It is noted however, that the actual surface remains mostly intact *i.e.* the surface porosity is quite low.

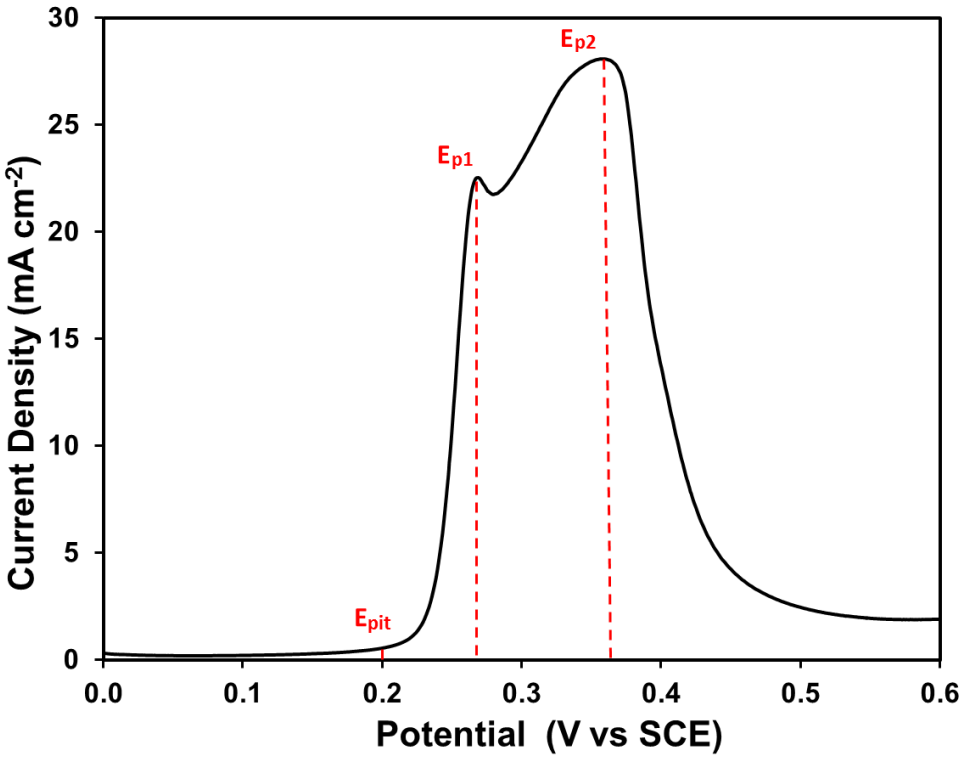

Fig. 1 LSV of InP in 5 mol dm^{-3} KOH. The potential was swept from 0.0 to E_{max} = 0.6 V (SCE) at 2.5 mV s^{-1}. Marked on the LSV are E_{pit}, the potential at which the first etch pits start to appear on the electrode surface, E_{p1}, the potential of the first current peak, and E_{p2}, the potential of the second current peak.

Due to limitations in carrier supply(31), etching is initially constrained to be normal to the electrode surface as was seen for the surface pits in Fig. 2. However, once the etch front has progressed by approximately the thickness of the depletion layer, pores begin to branch out from this initial pit and propagate along <111>A crystallographic directions(31, 33).

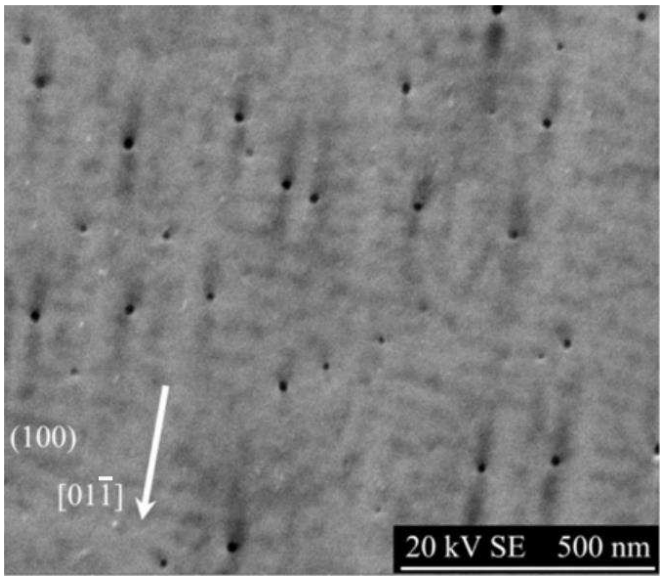

Fig. 2 SEM micrograph of an InP (100) surface following an LPS from 0.0 to 0.537 V (SCE). A number of etch pits are clearly visible on the electrode surface. Since the image was taken at 20 kV both the surface pits and some sub-surface features are shown.

Once crystallographically oriented pores have formed from the original etch pit, these pores continue to grow and branch, forming a complex network filled with electrolyte and etch products. As the pores branch, the number of actively growing pore tips increases, leading to a rapid increase in current in the LSV after E_{pit}. Each pore network may contain many actively growing (etching) pore tips but they are all connected to the bulk electrolyte via the original surface pit from which the initial pores formed. We call such a pore network (with only a single connection to the bulk electrolyte) a *porous domain*. These porous domains have the characteristic shape of a truncated tetrahedron(33) (due to their crystallographically oriented etching). This is illustrated schematically in Fig. 3 which shows the overall shape of a porous domain formed by pores etching exclusively along <111>A directions. This schematic also shows the porous domain cross sections that would be expected on different crystallographic planes. On the $(0\bar{1}1)$ plane an inverted triangle or "v-groove" shaped cross-section is expected. On the $(0\bar{1}\,\bar{1})$ plane a trapezoidalor "dove-tail" cross-section is expected.

The equivalent SEM cross-sections of actual porous domains are shown in Fig. 4. A $(0\bar{1}1)$ cross section is shown in Fig. 4a. It shows the characteristic v-groove domain shape. A similar domain, viewed on the $(0\bar{1}\,\bar{1})$ plane is shown in Fig. 4b. It shows the characteristic dove-tail domain shape. Both of these images also show that the porous domain is separated from the semiconductor surface by a surface layer of dense (*i.e.* low porosity) InP (labelled as A in each micrograph) which is penetrated at only one point, by the surface pit.

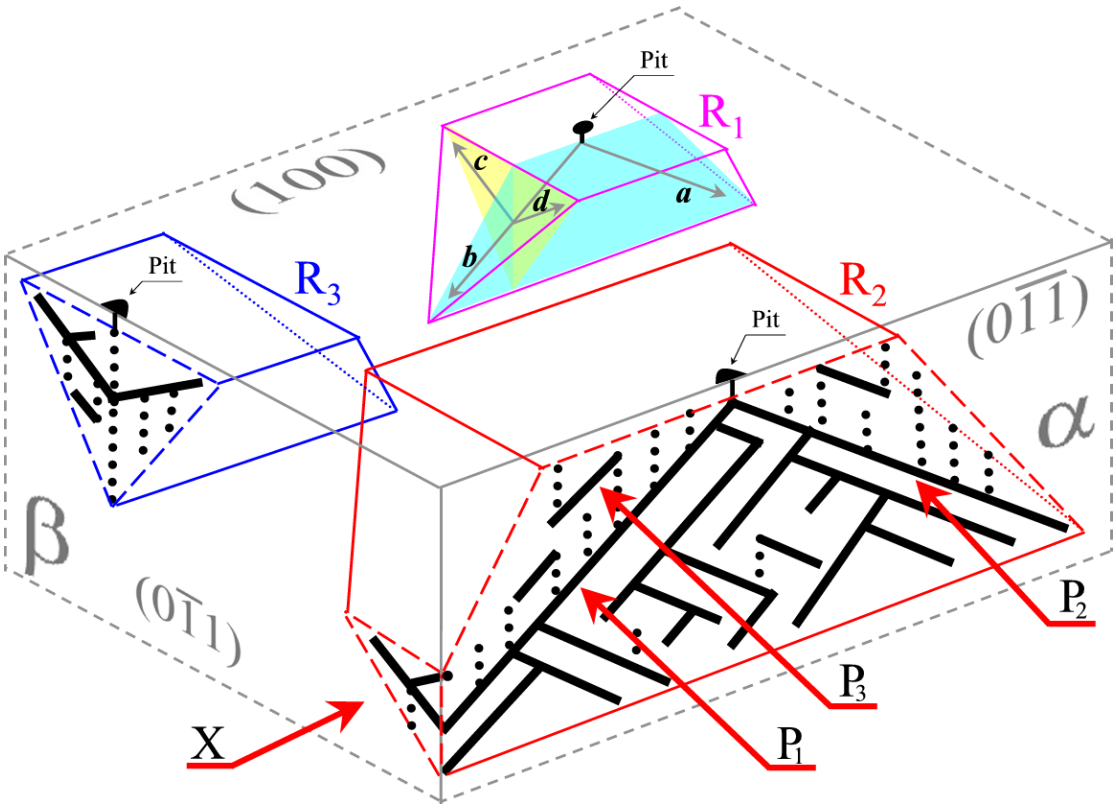

Fig. 3 Schematic of porous domains R_1, R_2 and R_3 beneath a (100) surface and cross sections in (0$\bar{1}$1) and (0$\bar{1}\bar{1}$) planes. Domains are separated from the surface by a thin layer of dense InP and each domain originates from a pit penetrating this layer. Pores are shown oriented along <111>A directions and the unique porous domain shapes that are seen in SEM cross sections are also shown.

As etching continues, these domains eventually merge with each other, which slows the increase in current, eventually resulting in a current peak at E_{p1}. Where the domains merge, the depletion layers surrounding individual pores overlap, resulting in a cessation of etching along that direction. Once all of the individual domains merge, a continuous porous layer is formed, which coincides with the trough in current seen just after E_{p1} in Fig. 1. However, pores at the base of the porous layer can continue to grow deeper in to the substrate, which results in the gradual thickening of the porous layer. This results in the pseudo-linear increase in current seen between the two current peaks in Fig. 1. This thickening continues until a second current peak is observed at E_{p2}, which is quickly followed by the cessation of porous layer growth(39).

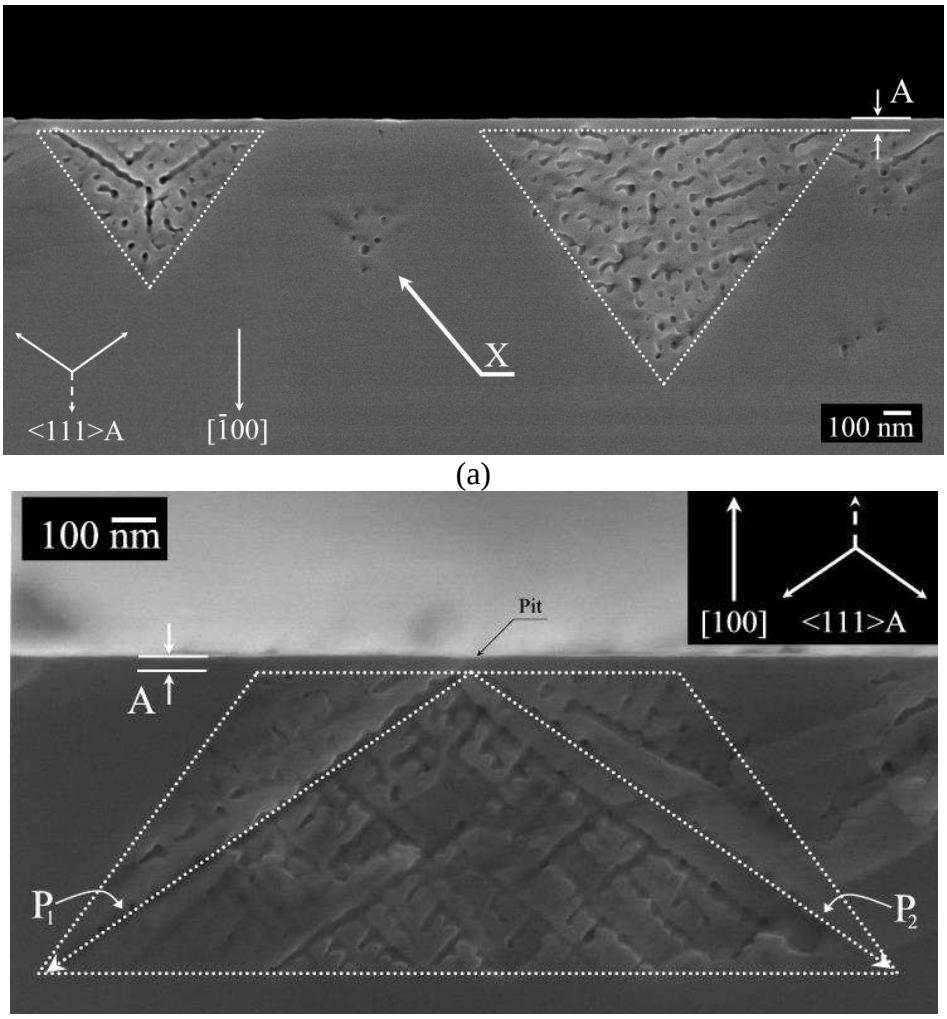

Fig. 4 SEM images of n-InP after an LPS from 0 V to 0.44 V (SCE) in 5 mol dm^{-3} KOH at 2.5 mV s^{-1}. (a) A cleaved $(0\bar{1}1)$ plane in which a characteristic v-groove porous domain cross section can be seen beneath a thin dense surface layer at A. (b) A cleaved $(0\bar{1}\,\bar{1})$ plane showing a characteristic dove tail domain cross section beneath a thin dense surface layer at A.

We have previously described how etching of porous layers in InP in KOH is a purely electrochemical process and this leads to some features which are not present in many other pore systems(31). As mentioned earlier, holes are supplied from the bulk of the semiconductor leading to narrow etch pits which penetrate a layer of dense InP. Since no chemical etching takes place, this surface layer of dense InP remains intact throughout the etching process. This was shown in Fig. 2 where the surface of a porous InP layer was shown to be almost completely intact, with the occasional surface pit offering the only hint at the sub-surface porosity. This creates a unique structure which consists of a porous layer sandwiched between two layers of dense InP; the dense surface layer and the bulk semiconductor. Furthermore, the structure obtained can be tailored by controlling the upper potential E_{max} in the LPS. In this way, isolated porous domains can be formed if

E_{max} is chosen such that $E_{pit}<E_{max}<E_{p1}$. The average size of these domains can also be tailored by stopping the potential sweep at an earlier or later time within this window.

In the next section, all of the porous samples shown have had their potential swept to $E_{pit}<E_{max}<E_{p1}$ as just described, so that the etching of individual porous domains can be studied.

Dissolution of porous layer

It is possible, at an elevated temperature, to chemically etch InP using a mixture of two parts (by volume) H_2SO_4 with three parts water (*i.e.* ~7.5 mol dm^{-3} H_2SO_4). Where the InP being etched has undergone a previous step to form domains of pores beneath the dense surface layer, it is observed that such chemical etching can result in a large number of bubbles emanating from the sample surface. These bubbles do not appear immediately but after a short period of time. SEM investigations of cleaned samples show that these bubbles corresponded to the rapid etching of the skeleton structure of InP in the porous domains. These bubbles could be PH_3 which may signify the progression of enhanced etching of the porous skeleton. Micrographs of the (100) surface of such a sample are shown in Fig. 5. In Fig. 5a an individual domain displaying the characteristic truncated tetrahedral domain shape can be seen. However in Fig. 5b two intersecting domains can be seen. In both images not alone has the internal InP structure been etched but the surface layer of dense InP has also been etched. This etching has made the truncated tetrahedral structures of the domains visible. Therefore, in Fig. 5a the elongation of the domain along one of the two <011> axes and the pointed vertices that are seen as symmetric sub-surface features are displayed. Where truncated tetrahedral shapes of domains are merged together along the $[01\bar{1}]$ axis there is a thick region (i.e. of up to several hundred nanometres, as shown at W in Fig. 5c) of dense InP that is between their point of merging and beneath the electrode-surface. Therefore when the porous skeleton and the dense surface layer have been etched, this thick region of dense InP becomes suspended above a void, as can be seen in Fig. 5b.

It can be seen in Fig. 5a and Fig. 5b that in both of the images the openings to the surface are not square, like the shape of the truncated domains just beneath the surface, but almost hexagonal. This may be due to etching outwards from the internal surfaces of the pores in the domains. It follows, that since the two primary pores grow downwards along the <111>A directions (towards the vertices of the domain) the surface pit should widen to a greater extent along these directions where there is enhanced etching due to the chemistry within the pores. Hence, a greater degree of etching results along the $[01\bar{1}]$ axis and void openings in the surface are hexagonal shaped.

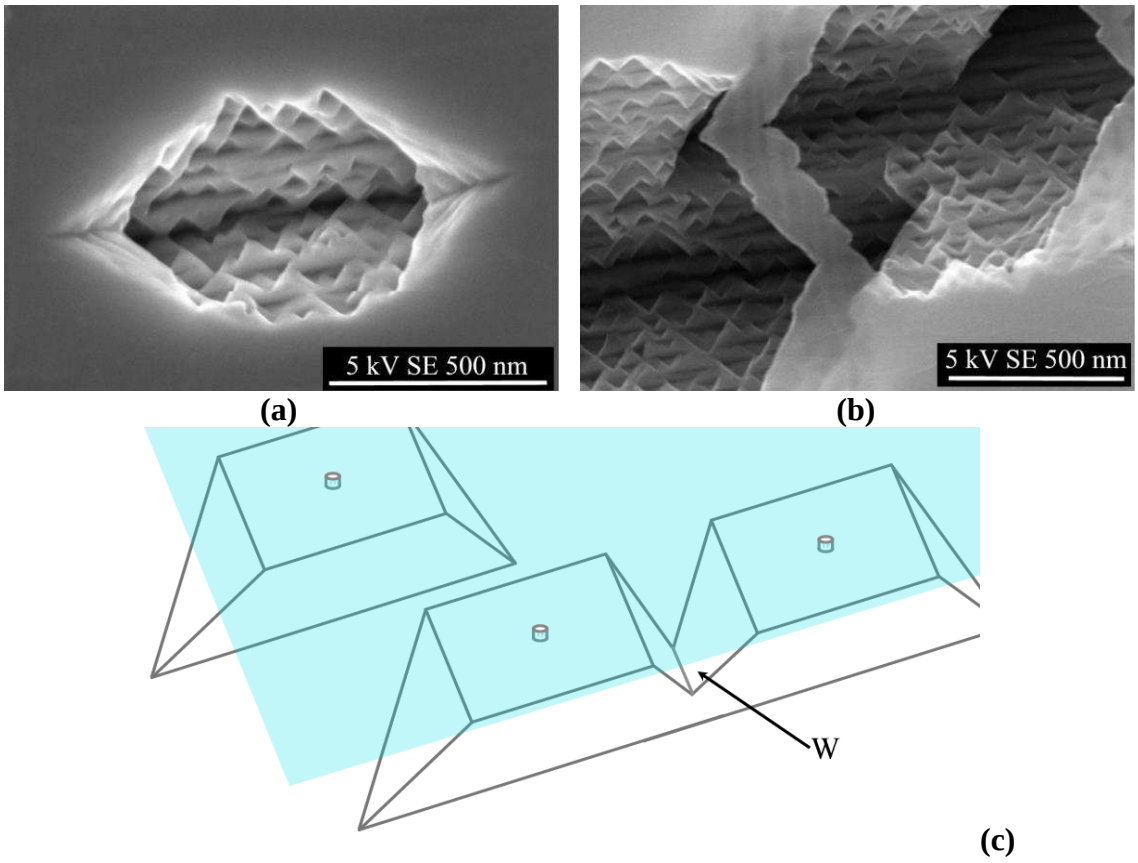

Fig. 5 SEM micrographs of (a) an individual porous domain and (b) two intersecting domains that have been etched by ~7.5 mol dm^{-3} H_2SO_4 at 70°C for 150 s. The sample was taken directly from room temperature water and placed in the H_2SO_4 solution. (c) A schematic representation of the individual and intersecting porous domain outlines prior to etching is shown and a volume of bulk InP that is surrounded due to the merging of two domains is indicated at W.

Where the InP being etched contains porous domains the inter-pore regions (pore walls) etch much more quickly than the bulk. The enhanced rate of etching within the porous structure may be due to the combination of two effects. The first effect is due to the surface-area to volume ratio being greater for the pore walls than for the dense surface layer of InP. This results in the build-up of a large number of chemical products within the porous domain. The second effect may therefore be due to enhancement of the etching rate within the porous domains by the chemical products trapped inside, thus changing the chemistry within the domains. Furthermore, such an effect – that is dependent on an initiation time, during which the reactants required for enhanced etching accumulate – would explain the absence of bubbles when the samples are initially placed in the H_2SO_4 solution. Therefore it is likely (since only ~20% of the volume of each domain is porous and ~80% of the domain is InP) that the accumulation of products in the enclosed regions of the porous domain results in a change in the chemistry within the domain and a subsequent enhancement in etching of the pore walls.

If it is the case that the porous structures undergo enhanced etching, it follows that control of etching time could lead to structures such as those shown in Fig. 6. In this

schematic it is shown that a layer of dense InP, ~40 nm thick, that is suspended over a void can be formed if an etching mechanism preferentially removes the internal domain skeleton while leaving the surface layer intact.

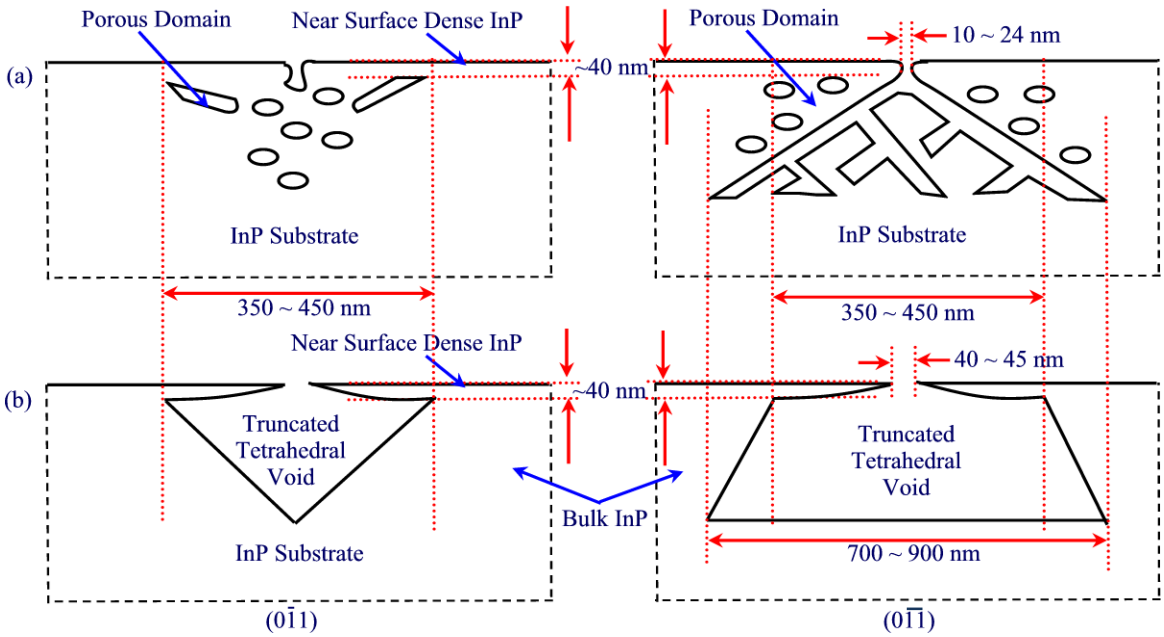

Fig. 6 Schematic showing the layout of (a) a domain of pores grown by anodization of InP and (b) the void created by the chemical removal of the internal InP skeleton of such a domain. Such a process would provide isolated and suspended regions, of thicknesses ~40 nm, above volumes void of semiconductor.

Effect of H_2SO_4 Concentration on Etching

Several concentrations ranging from 1 mol dm^{-3} H_2SO_4 to concentrated H_2SO_4 were tested at room temperature. These experiments were performed so as to tailor the etching of the skeleton of the porous domain with the aim of realizing structures similar to those shown in Fig. 6. During all of these experiments there was no observation of bubbles emanating from the sample surfaces. In the previous experiments, which were carried out at elevated temperatures, the presence of bubbles emanating from the surface coincided with the etching of the skeleton of the porous domain. Therefore the lack of bubbles suggests that no significant etching occurs in H_2SO_4 solutions at room temperature, regardless of concentration. Further examination by SEM surface and cross-sectional analyses confirmed that no noticeable etching of the porous skeleton occurred during the time the samples were held in solution at room temperature. This therefore suggests that the etching mechanism and the production of bubbles are inextricably linked and interdependent. Furthermore, it suggests that elevated temperature is essential for the etching mechanism. A possible reason for this may be that, at low temperatures, the etching of InP by H_2SO_4 solution is slow and the products responsible for the enhanced etching have sufficient time to escape from the confined regions of the porous domains

and therefore never accumulate in sufficient concentrations for enhanced etching to occur.

Effect of H_2SO_4 Temperature on Etching

The effect of temperature on the chemical etching of porous structures in concentrated H_2SO_4 solutions (~7.5 mol dm^{-3}) was also investigated. Prior to etching, the samples were made porous through anodizing in 5 mol dm^{-3} KOH via an LPS from 0.0 to E_{max} = 0.25 V (*i.e.* $E_{pit}<E_{max}<E_{p1}$ so that some isolated domains were obtained) at 2.5 mV s^{-1}. These samples were then rinsed with water prior to steeping in water overnight. Each sample was then steeped in H_2SO_4 solution for 90 seconds at bath temperatures ranging from 20°C to 90°C.

Above 60°C bubbles were found to emanate from the sample surface during steeping with a large amount of bubbles emanating above 70°C. As mentioned earlier, the observation of bubbles coincides with the chemical etching of InP. Therefore etching of InP in ~7.5 mol dm^{-3} H_2SO_4 does not seem to occur unless the solution temperature is 60°C or higher. Fig. 7 shows SEM images of a sample etched at 60°C for 90 s. Despite the observation of bubbles during etching, very little etching of the porous domain has occurred. A slight increase in the pore width (from 29 nm to 38 nm) and in the average pit diameter (from 15 nm to 20 nm) is observed in Fig. 7a and Fig. 7b, respectively.

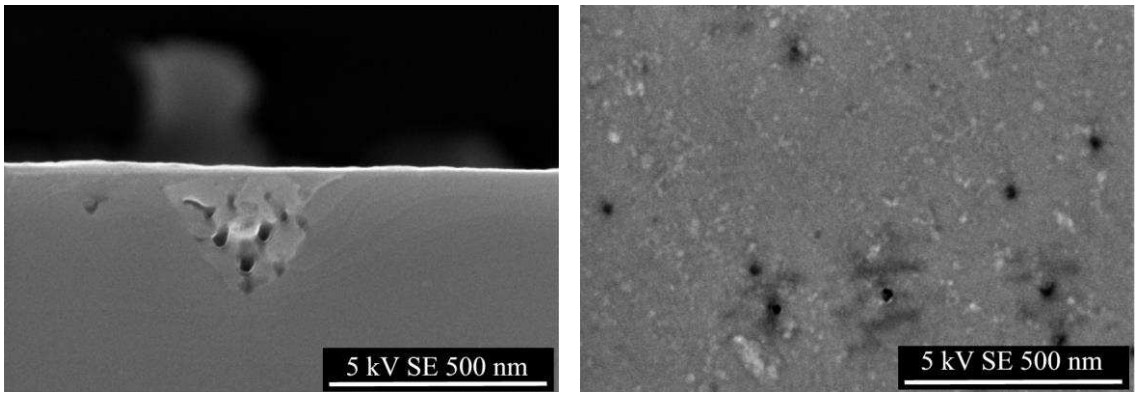

(a) **(b)**

Fig. 7 SEM (a) $(0\bar{1}1)$ cross-sectional and (b) (100) surface views of InP containing porous domains created by LPS in KOH that have been chemically etched in 7.5 mol dm^{-3} H_2SO_4 for 90 s at 60°C.

In contrast to Fig. 7, Fig. 8 shows an SEM image of a sample that has been 'over-etched'. The sample was etched for the same time of 90 s but at a higher temperature of 80°C. As shown in Fig. 8a these conditions result in the removal of most of the dense surface layer leaving only the remnants of the original surface in regions were no porous domains had been formed. This etching of the dense surface layer is also seen in the cross-sectional image of Fig. 8b. It can be observed in this image that the skeletons of the porous domains have been etched away and that the etching has also resulted in the non-uniform etching of the triangular outline of the domains. While an increase in temperature from 60°C to 80°C is expected to lower the energy barrier for chemical

reaction and thereby enhance the reaction kinetics, the enormous increase in the amount of etching suggests that the etching process is also being enhanced by the onset of an additional mechanism (as alluded to earlier in the text). If the presence of etch products within the pores is responsible for the enhancement of the reaction, any increase in the etch rate would be self-enhancing, since it would result in the trapping of further chemical products within the porous structure. Therefore it seems very plausible that the rapid increase of etch rate with temperature is due to such a change of chemistry within the domains.

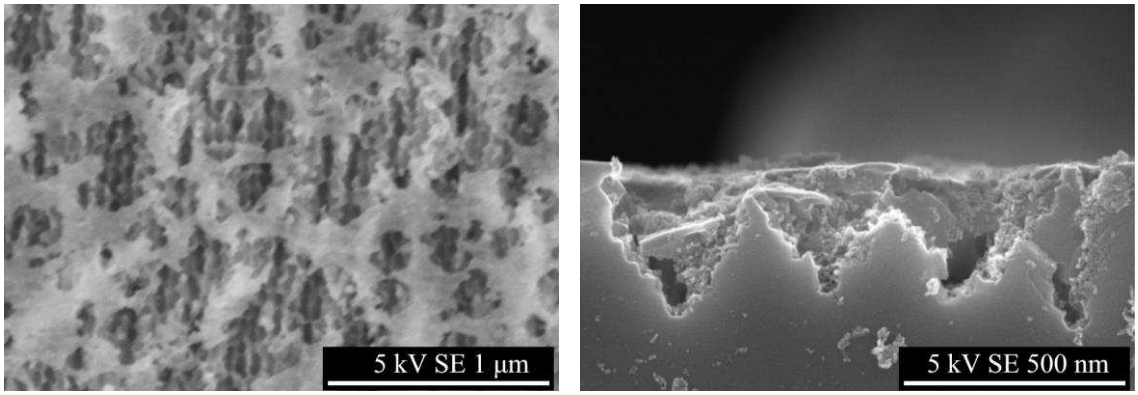

(a) **(b)**

Fig. 8 SEM (a) (100) surface and (b) $(0\bar{1}1)$ cross-sectional views of InP containing porous domains created by LPS in KOH that have been chemically etched in 7.5 mol dm^{-3} H_2SO_4 for 90 s at 80°C.

By choosing an intermediate temperature of 70°C it is possible to etch the internal skeleton structure completely, while leaving the dense surface layer of isolated domains almost fully intact. Fig. 9 is a $(0\bar{1}1)$ SEM cross-section from such an experiment. It can be observed that the dense surface layer and the triangular outline of the domain are still intact but that the internal skeleton structure is completely removed. It can also be seen that the etching process is more controlled at this temperature with no over-etching of the domain outline being seen. The majority of the isolated domain cross-sections observed for the experiment shown in Fig. 9 ranged from 350 to 450 nm and measurements of the surface-pit diameter for these domains showed an increase to between 40 and 45 nm (from between 10 and 24 nm prior to etching).This is in contrast with the less controlled etching at the higher temperature (Fig. 8b).

This controlled etching is also seen in the image shown earlier in Fig. 5 and is maintained for extended durations of etching, up to the removal of the dense surface layer, verifying that the etching is due to a change in chemistry within the porous domains. That is to say that when the dense surface layer is etched away, from the inside outwards, the unique chemical mixture that has built up within the domain is released and the etching is no longer enhanced by the etch products. This results in the cessation of etching, hinted at by the observation that bubbles stop emanating from the sample. It follows that the process is self-limiting and can therefore be used for highly reproducible formation of tetrahedral voids in the InP surface. It also follows that the amount of etching of the porous domain and dense surface layer can be controlled by controlling the duration of etching to any time up to times corresponding to the self-limiting case.

Increasing the temperature past 70°C results in an increase in the aggressiveness and lack of control of the etching resulting in highly disordered etching of the porous structures (as seen in Fig. 8b).

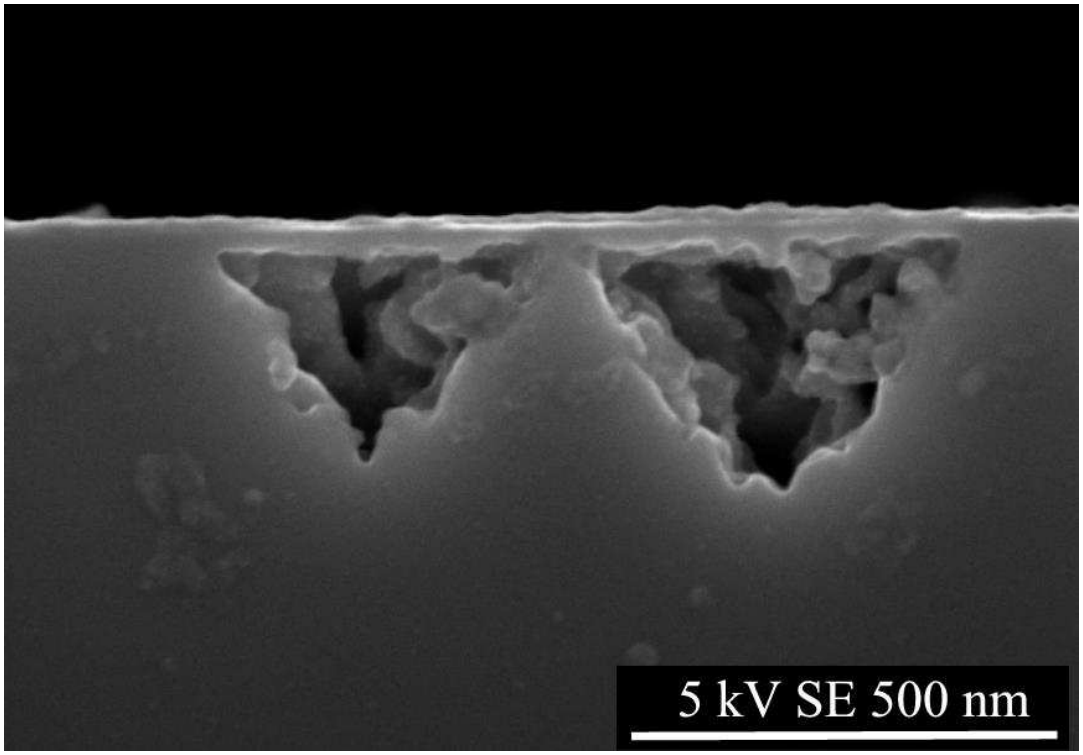

Fig. 9 SEM $(0\bar{1}1)$ cross-section of porous domains in InP that have been etched in 7.5 mol dm^{-3} H_2SO_4 for 90 s at 70°C displaying and etched interior and an intact dense surface layer.

It can be clearly seen in Fig. 9 that there are regions of unetched semiconductor beneath the dense surface layer and outside of the original outlines of the domains of pores. Therefore many of the domains have not begun to merge together but due to the non-uniform nucleation and distribution of surface pits some domains begin to merge together much sooner than others. Fig. 10 shows an SEM cross-section of several domains from the same sample shown in Fig. 9. Due to the proximity of the surface pits of these domains, the domains have merged together and therefore the voids created during chemical etching overlap each other. It can be observed in the image that, although the triangular nature of the domain outlines can still be seen, the dense surface layer (at D) has been etched considerably resulting in its break-up. This type of etching, where the near-surface layer breaks up, only occurred where the domains were merged with each other. It can also be observed in this image that the etching has a slightly greater degree of disorder than in Fig. 9, even though they belong to the same experiment. Possible reasons for this include the trapping of products in the slightly narrower pores that form at the edge of merging domains. Any such trapping would result in magnification of the chain reaction, leading to more-enhanced, more-disordered etching. Furthermore, the structural weakness of a dense surface layer that spans more than one domain could result in the collapse of the suspended layer.

This type of overetching may be prevented by greater control of porous domain formation during anodisation. As has been noted in previous publications(31, 54), the pits that form at E_{pit} preferentially form at defects. Therefore the porous domains could be evenly distributed by patterning the InP surface with a regular distribution of defects using a focused ion beam (FIB) or by forming a regular array of etch pits on the surface using a photolithographically patterned etching process. In such a manner, controlled fabrication of complex devices such as wave guides or gas sensors could be realised in InP, using only a few simple chemical/electrochemical steps to produce sub-surface structures similar to those discussed above. Since anodisation results in similar pore formation in other semiconductors, this technique may be applicable to a range of materials including GaAs, InSb and GaP. Indeed, research on such materials may elucidate the underlying chemical mechanism behind the selective dissolution of the porous skeleton.

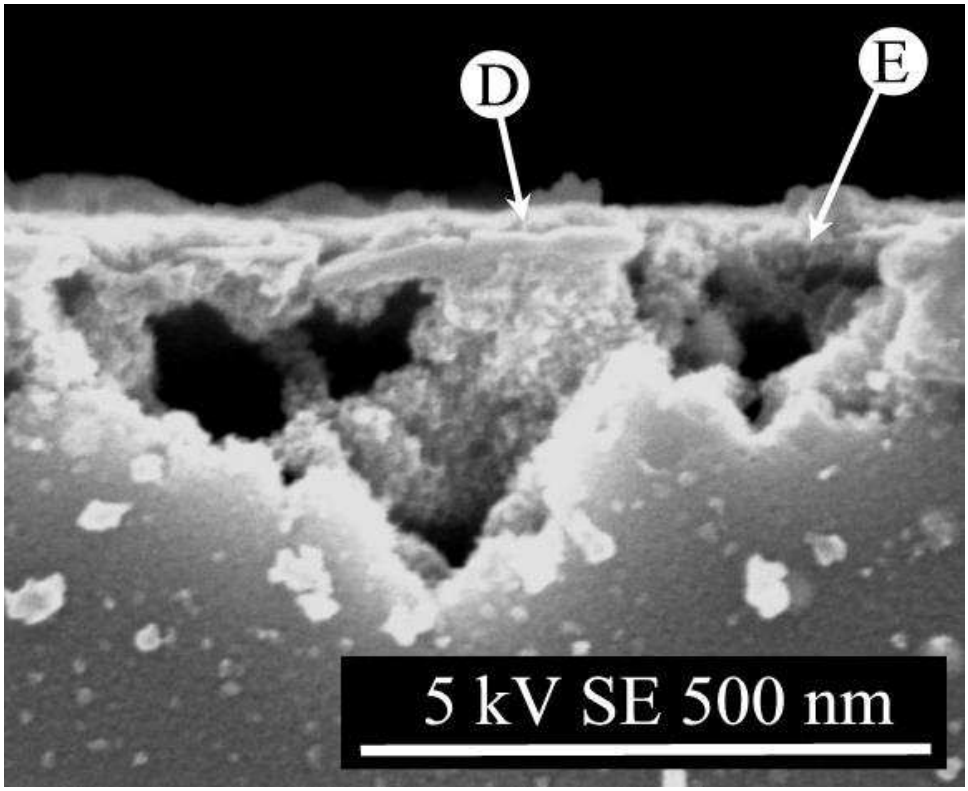

Fig. 10 SEM $(0\bar{1}1)$ cross-section of InP containing porous domains that have been etched in 7.5 mol dm^{-3} H_2SO_4 for 90 s at 70°C. The cross-section image shows a damaged near-surface layer (at D) with some of the layer completely removed (at E).

Conclusions

During the early stages of electrochemical pore formation in InP in KOH, isolated domains of pores in the shape of truncated tetrahedra can be formed beneath a thin layer of dense (*i.e.* low porosity) InP. The porous structures formed can be chemically etched by 7.5 mol dm^{-3} H_2SO_4 at temperatures above 60°C. It follows that the process of etching

these domains allows for the engineering of suspended 40-nm-thick layers above truncated tetrahedral voids. Greatest control of the etching process occurs at temperatures near 70°C and the degree of etching can be controlled by the etching time. The mechanism of the chemical etch seems to be dependent on the trapping of etch products within the porous structure resulting in the internal InP skeleton of the porous domains being etched by the H_2SO_4 at a higher rate than the surface layer of dense InP. It follows that once the dense surface layer that is containing these etch products is itself etched, the products diffuse away and the etching stops; *i.e.* the mechanism is self-limiting. It follows that this new technique can be used for the controlled formation of a range of structures including suspended nano-films and truncated tetrahedral voids. Such a technique may be a very useful tool in the fabrication of devices based on InP and it may be possible to extend the technique to the fabrication of free-standing InP nanofilms.

Acknowledgments

R. P. Lynch and N. Quill would like to thank the Irish Research Council (IRC) for PhD scholarships to perform this research. R. P. Lynch acknowledges a joint IRC - Marie Skłodowska Curie Fellowship under grant no. INSPIRE PCOFUND-GA-2008-229520. The authors would also like to acknowledge the support of the Tyndall National Institute through National Access Programme Funding.

References

1. R. L. Smith and S. D. Collins, *J. Appl. Phys.*, **71**, R1 (1992).
2. S. Langa, J. Carstensen, M. Christophersen, H. Foll and I. M. Tiginyanu, *Appl. Phys. Lett.*, **78**, 1074 (2001).
3. G. Oskam, A. Natarajan, P. C. Searson and F. M. Ross, *Appl. Surf. Sci.*, **119**, 160 (1997).
4. S. Langa, J. Carstensen, I. M. Tiginyanu, M. Christophersen and H. Foll, *Electrochem. Solid-State Lett.*, **4**, G50 (2001).
5. S. Langa, I. M. Tiginyanu, J. Carstensen, M. Christophersen and H. Foll, *Electrochem. Solid-State Lett.*, **3**, 514 (2000).
6. P. Schmuki, J. Fraser, C. M. Vitus, M. J. Graham and H. S. Isaacs, *J. Electrochem. Soc.*, **143**, 3316 (1996).
7. P. Schmuki, D. J. Lockwood, H. J. Labbe and J. W. Fraser, *Appl. Phys. Lett.*, **69**, 1620 (1996).
8. L. Santinacci, A.-M. Gonçalves, M. Bouttemy and A. Etcheberry, *J. Solid State Electrochem.*, **14**, 1177 (2010).
9. A. Eb, A.-M. Gonçalves, L. Santinacci, C. Mathieu and A. Etcheberry, *Comptes Rendus Chimie*, **11**, 1023 (2008).
10. L. Santinacci, M. Bouttemy, I. Gerard and A. Etcheberry, *ECS Trans.*, **19**, 313 (2009).
11. B. H. Erné, D. Vanmaekelbergh and J. J. Kelly, *Adv. Mater.*, **7**, 739 (1995).

12. J. G. Rivas, A. Lagendijk, R. W. Tjerkstra, D. Vanmaekelbergh and J. J. Kelly, *Appl. Phys. Lett.*, **80**, 4498 (2002).
13. M. Christophersen, J. Carstensen, A. Feuerhake and H. Föll, *Mat. Sci. Eng., B,* **69-70**, 194 (2000).
14. N. Quill, R. P. lynch, C. O'Dwyer and D. N. Buckley, *ECS Trans.*, **50**, 131 (2013).
15. N. Quill, R. P. Lynch, C. O'Dwyer and D. N. Buckley, *ECS Trans.*, **50**, 377 (2013).
16. A. M. Goncalves, L. Santinacci, A. Eb, I. Gerard, C. Mathieu and A. Etcheberry, *Electrochem. Solid-State Lett.*, **10**, D35 (2007).
17. R. P. Lynch, C. O'Dwyer, D. N. Buckley, D. Sutton and S. Newcomb, *ECS Trans.*, **2**, 131 (2006).
18. S. Ronnebeck, J. Carstensen, S. Ottow and H. Foll, *Electrochem. Solid-State Lett.*, **2**, 126 (1999).
19. P. Schmuki, L. E. Erickson, D. J. Lockwood, J. W. Fraser, G. Champion and H. J. Labbe, *Appl. Phys. Lett.*, **72**, 1039 (1998).
20. V. Lehmann and H. Foll, *J. Electrochem. Soc.*, **137**, 653 (1990).
21. T. Unagami, *J. Electrochem. Soc.*, **127**, 476 (1980).
22. J. Cartensen, M. Christophersen and H. Foll, *Mat. Sci. Eng., B,* **69-70**, 23 (2000).
23. F. M. Ross, G. Oskam, P. C. Searson, J. M. Macaulay and J. A. Liddle, *Philos. Mag. A*, **75**, 525 (1997).
24. M. J. J. Theunissen, *J. Electrochem. Soc.*, **119**, 351 (1972).
25. M. I. J. Beale, J. D. Benjamin, M. J. Uren, N. G. Chew and A. G. Cullis, *J. Cryst. Growth*, **73**, 622 (1985).
26. P. Allongue and C. H. de Villeneuve, *Appl. Phys. Lett.*, **67**, 941 (1995).
27. V. Lehmann and U. Gosele, *Appl. Phys. Lett.*, **58**, 856 (1991).
28. J.-N. Chazalviel, F. Ozanam, N. Gabouze, S. Fellah and R. B. Wehrspohn, *J. Electrochem. Soc.*, **149**, C511 (2002).
29. X. G. Zhang, *J. Electrochem. Soc.*, **138**, 3750 (1991).
30. X. G. Zhang, *J. Electrochem. Soc.*, **151**, C69 (2004).
31. R. P. Lynch, N. Quill, C. O'Dwyer, S. Nakahara and D. N. Buckley, *Phys. Chem. Chem. Phys.*, **15**, 15135 (2013).
32. L. Santinacci, I. Gerard, M. Bouttemy, M. Marques and A. Etcheberry, *ECS Trans.*, **16**, 411 (2008).
33. R. P. Lynch, C. O'Dwyer, N. Quill, S. Nakahara, S. B. Newcomb and D. Noel Buckley, *J. Electrochem. Soc.*, **160**, D260 (2013).
34. R. P. Lynch, C. O'Dwyer, D. Sutton, S. B. Newcomb and D. N. Buckley, *ECS Trans.*, **6**, 355 (2007).
35. C. O'Dwyer, D. N. Buckley, D. Sutton, M. Serantoni and S. B. Newcomb, *J. Electrochem. Soc.*, **154**, H78 (2007).
36. N. Quill, R. P. lynch, C. O'Dwyer and D. N. Buckley, *ECS Trans.*, **50**, 143 (2013).
37. C. O'Dwyer, D. N. Buckley, D. Sutton and S. B. Newcomb, *J. Electrochem. Soc.*, **153**, G1039 (2006).
38. R. P. Lynch, M. Dornhege, P. S. Bodega, H. H. Rotermund and D. N. Buckley, *ECS Trans.*, **6**, 331 (2007).

39. R. P. Lynch, N. Quill, C. O'Dwyer, M. Dornhege, H. H. Rotermund and D. N. Buckley, *ECS Trans.*, **53**, 65 (2013).
40. T. Sato, A. Mizohata, N. Yoshizawa and T. Hashizume, *Applied Physics Express*, **1**, 051202 (2008).
41. T. Sato, T. Fujino, A. Mizohata and T. Hashizume, in *E-MRS Fall Meeting 2007, Symposium B*, Warsaw (2007).
42. A. Salehi and D. Jamshidi Kalantari, *Sens. Actuators, B*, **122**, 69 (2007).
43. I. M. Tiginyanu, I. V. Kravetsky, S. Langa, G. Marowsky, J. Monecke and H. Föll, *Phys. Stat. Sol., A*, **197**, 549 (2003).
44. H. Tsuchiya, M. Hueppe, T. Djenizian, P. Schmuki and S. Fujimoto, *Sci. Tech. Adv. Mater*, **5**, 119 (2004).
45. G. Flamand and J. Poortmans, *Phys. Stat. Sol., A*, **202**, 1611 (2005).
46. H. Foll, J. Cartensen and S. Frey, *J. Nanometer.*, 1 (2006).
47. V. Kochergin and H. Foell, *Materials Science and Engineering: R: Reports*, **52**, 93 (2006).
48. A. Salehi, A. Nikfarjam and D. J. Kalantari, *Sens. Actuators, B*, **113**, 419 (2006).
49. E. H. M. Camara, C. Pijolat, J. Courbat, P. Breuil, D. Briand and N. F. de Rooij, *Transducers and Eurosensors '07* (2007).
50. J. H. Kwon, S. H. Lee and B. K. Ju, *J. Appl. Phys.*, **101**, 104515 (2007).
51. J. Mizsei, *Thin Solid Films*, **515**, 8310 (2007).
52. B. H. Erne, D. Vanmaekelbergh and J. J. Kelly, *J. Electrochem. Soc.*, **143**, 305 (1996).
53. R. W. Tjerkstra, J. Gomez Rivas, D. Vanmaekelbergh and J. J. Kelly, *Electrochem. Solid-State Lett.*, **5**, G32 (2002).
54. P. Schmuki, U. Schlierf, T. Herrmann and G. Champion, *Electrochim. Acta*, **48**, 1301 (2003).